Inorg. Chem. **2008**, *47*, 11519−11526

Photochemical Reactions of *fac*-[Mn(CO)$_3$(phen)imidazole]$^+$: Evidence for Long-Lived Radical Species Intermediates

Inara de Aguiar,[†] Simone D. Inglez,[‡] Francisco C. A. Lima,[‡] Juliana F. S. Daniel,[†] Bruce R. McGarvey,[§] Antônio C. Tedesco,[||] and Rose M. Carlos*[,†]

Departamento de Química, Universidade Federal de São Carlos, CP 676, 13565-905, São Carlos, SP, Brasil, Instituto de Química de São Carlos, Universidade de São Paulo, CP 780, 13650-970, São Carlos, SP, Brasil, Faculdade de Filosofia, Ciências e Letras de Ribeirão Preto, Universidade de São Paulo, Ribeirão Preto, SP, Brasil, and Department of Chemistry and Biochemistry, University of Windsor, Windsor Ontario, Canada N9B 3P4

Received January 31, 2008

The electronic absorption spectrum of *fac*-[Mn(CO)$_3$(phen)imH]$^+$, *fac*-**1** in CH_2Cl_2 is characterized by a strong absorption band at 378 nm (ε_{max} = 3200 mol^{-1} L cm^{-1}). On the basis of quantum mechanical calculations, the visible absorption band has been assigned to ligand-to-ligand charge-transfer (LLCT, im→phen) and metal-to-ligand charge-transfer (MLCT, Mn→phen) charge transfer transition. When *fac*-**1** in CH_2Cl_2 is irradiated with 350 nm continuous light, the absorption features are gradually shifted to represent those of the meridional complex *mer*-[Mn(CO)$_3$(phen)imH]$^+$, *mer*-**1** (λ_{max} = 556 nm). The net photoreaction under these conditions is a photoisomerization, although, the presence of the long-lived radical species was also detected by ^{1}H NMR and FTIR spectroscopy. 355 nm continuous photolysis of *fac*-**1** in CH_3CN solution also gives the long-lived intermediate which is readly trapped by metylviologen (MV^{2+}) giving rise to the formation of the one-electron reduced methyl viologen ($MV^{\bullet+}$). The UV−vis spectra monitored during the slow (45 min) thermal back reaction exhibited isosbestic conversion at 426 nm. On the basis of spectroscopic techniques and quantum mechanical calculations, the role of the radicals produced is analyzed.

I. Introduction

The imidazole group of histidine is of major importance in biology,[1] acting in enzymatic reactions as a proton-transfer mediator and in organizing the active centers of enzymes.[2] Thus, histidine residues appear in a wide variety of redox active and metabolic enzymes, particularly those with Cu(II), Zn(II), Mn(II), or Fe(II) centers.[3] Manganese, for example, is an essential element for the process of photosynthetic water oxidation.[4] For these reasons, the studies of the manganese-imidazole interaction in terms of affinity properties and the manner in which the imidazole moiety will affect the redox properties and stabilities of the oxidation states of the

* To whom correspondence should be addressed. E-mail: rosem@dq.ufscar.br.
[†] Universidade Federal de São Carlos.
[‡] Instituto de Química de São Carlos, Universidade de São Paulo.
[§] University of Windsor.
[||] Faculdade de Filosofia, Ciências e Letras de Ribeirão Preto, Universidade de São Paulo.

(1) (a) Hasegawa, K.; Ono, T.; Noguchi, T. *J. Phys. Chem. B* **2000**, *104*, 4253–4265. (b) Blomberg, F.; Maurer, W.; Ruterjans, H. *J. Am. Chem. Soc.* **1977**, *99*, 8149–8159. (c) AshiKawa, I.; Itoh, K. *Biopolymers* **1979**, *18*, 1859–1876. (d) Gorren, A. C. F.; denBlaauwen, T.; Canters, G. W.; Hopper, D. J.; Duine, J. A. *FEBS Lett.* **1996**, *381*, 140–142.
(2) (a) Sibert, R.; Josowicz, M.; Porcelli, F.; Veglia, G.; Range, K.; Barry, B. A. *J. Am. Chem. Soc.* **2007**, *129*, 4393–4400. (b) Roy, A.; Taraphder, S. *J. Phys. Chem. B* **2007**, *111*, 10563–10576. (c) Warshel, A.; Sussman, F.; King, G. *Biochemistry* **1986**, *25*, 8368–8372. (d) Hays, A. M. A.; Vassiliev, I. R.; Golbeck, J. H.; Debus, R. J. *Biochemistry* **1998**, *37*, 11352–11365.
(3) (a) Unger, Y.; Taige, M. A.; Ahrens, S.; Strassner, T. *Inorg. Chim. Acta* **2007**, *360*, 3699–3704. (b) Altun, Y.; Koseoglu, F. O. *J. Solution Chem.* **2005**, *34*, 213–231. (c) Kropidlowska, A.; Chojnacki, J.; Becker, B. O. *J. Inorg. Biochem.* **2007**, *101*, 578–584. (d) Abuskhuna, S.; McCann, M.; Briody, J.; Devereux, M.; McKee, M. *Polyhedron* **2004**, *23*, 1731–1737. (e) Manchanda, R.; Brudvig, G. W.; Crabtree, R. H. *Coord. Chem. Rev.* **1995**, *144*, 1–38.
(4) (a) Tommos, C.; Babcock, G. T. *Biochim. Biophys. Acta* **2000**, *1458*, 199–219. (b) Manchanda, A. R.; Brudvig, G. W.; Crabtree, R. H. *Coord. Chem. Rev.* **1995**, *144*, 1–38. (c) Messinger, J. *Biochim. Biophys. Acta* **2000**, *1459*, 481–488. (d) Debus, R. J. *Biochim. Biophys. Acta* **2001**, *1503*, 164–186.
(5) (a) Lahiri, J.; Fate, G. D.; Ungashe, S. B.; Groves, J. T. *J. Am. Chem. Soc.* **1996**, *118*, 2347–235. (b) Ye, B. H.; Mak, T.; Willians, I. D.; Li, X. Y. *Chem. Commun.* **1997**, *18*, 1813–1814. (c) Ferreira, A. D. Q.; Vinhado, F. S.; Iamamoto, Y. *J. Mol. Catal. A: Chem.* **2006**, *243*, 111–119. (d) Mohajer, D.; Karimipour, G.; Bagherzadeh, M. *New J. Chem.* **2004**, *28*, 740–747.

10.1021/ic8002004 CCC: $40.75 © 2008 American Chemical Society
Published on Web 11/01/2008

manganese center are biologically of great importance and involve applications in the areas of medicine, biology, and materials science.[5]

To study these fast electron transfer processes we could employ a compound that has relatively low thermal reactivity but is photochemically active to give imidazole radicals when subjected to electronic excitation.[6] Thus, research in this laboratory is concerned about applying electrochemical and photochemical techniques to map the electron transfer properties and chemical reactivity of Mn(I) complexes as potential inorganic redox agents.

In this context, an earlier report from this laboratory describes the synthesis, electrochemical characterizations, and continuous photolysis experiments of a series of manganese(I) carbonyl complexes.[6,7] In that report, it was shown that electrochemical oxidation and irradiation into the visible absorption band of *fac*-$[Mn(CO)_3(L'\text{-}L')(L)]^{0/+}$ [L′-L′ = 1,2-bis(diphenylphosphino)ethane (dppe) or 1,10-phenanthroline (phen) and L = bromide, triflate, imidazole, isonicotinamide, or N-(2-hydroxyethyl)isonicotinamide] resulted in *fac*- to *mer*- isomerization.[7]

To probe the spectra and dynamics of possible reactive intermediates on the excited states, we report the detailed investigation of the photochemical properties of *fac*-$[Mn(phen)(CO)_3(imH)]^+$, *fac*-**1**, as studied by continuous and flash photolysis experiments using spectroscopic (time-resolved optical, UV−vis, FTIR, ^1H, ^{13}C NMR) techniques. To rationalize the experimental data, a theoretical investigation, based on density-functional theory (DFT) calculations in CH_2Cl_2 has also been performed.

II. Experimental Section

Materials. *fac*-$[Mn(CO)_3(phen)(imH)]^+$ was prepared according to literature procedures.[6] All spectroscopic measurements were carried out in spectroscopically pure solvents.

Spectroscopic Techniques. Optical spectra were recorded on a Varian model Cary 500 NIR spectrophotometer. The FTIR spectra were measured in CaF_2 windows in CH_2Cl_2 solution on a Bomem-Michelson 102 spectrometer in the 4000−1000 cm^{-1} region. CHN elemental analyses were performed on an EA 1110 CHNS-O Carlo Erba Instrument in the Microanalytical Laboratory at Universidade Federal de São Carlos (SP).

NMR data were acquired using a Bruker DRX-400 Spectrometer. Samples were prepared for ^1H experiments under an inert atmosphere and analyzed at room temperature using deuterated solvent (CD_2Cl_2). All chemical shifts (δ) are given in ppm units with reference to the hydrogen signal of the methyl group of tetramethylsilane (TMS) as internal standard and the coupling constants (J) are in Hz.

Continuous Photolysis. Monochromatic irradiations at 350 nm were generated either using a 200 W Xenon lamp in an Oriel model 68805 Universal Arc Lamp source, selected with an appropriate interference filter (Oriel), or with an RMR-600 model Rayonet Photochemical reactor using RMR-3500 lamps. Experiments were carried out at room temperature in 1.0 cm path length 4 side quartz cells capped with a rubber septum. Magnetically stirred solutions ($\sim 10^{-4}-10^{-2}$ mol L^{-1} initial complex concentration) were under dinitrogen. Potassium (tris-oxalate)ferrate(III), used in actinometry at 350 nm, was prepared according to Calvert and Pitts.[8] The progress of the photoreaction was monitored by UV−vis, FTIR, and ^1H NMR spectra.

Flash-Photolysis. Time-resolved optical spectra were obtained using a laser flash-photolysis apparatus containing a Continuum Q-switched Nd:YAG laser (Continuum, Santa Clara, CA) with excitation provided by the third harmonic at $\lambda = 355$ nm. The pulse length was 8 ns, the beam diameter incident on sample was 6 mm, and the repetition rate was 10 Hz. The laser pulse was set up to 8 mJ per pulse in the photobleaching studies measured with a Field Master power meter with L-30V head. The growth-decay kinetics were measured at a single wavelength using a monochromator (M300 from Bentham) and a photomultiplier (Hamamatsu, model R928P). Transient decays were averaged using a Tetronix TDS 340A digital oscilloscope. Digitized kinetics data were transferred to a personal computer (PC) for the analysis with software supplied by Edinburgh Instruments.

Quenching Experiments. All sample solutions were prepared in a vacuum line with meticulous care to avoid oxygen contamination. A glass apparatus used for the present study consists of a round-bottomed vessel (1 mL) connected to a quartz cell (1 cm optical length) fixed to a gas/vacuum manifold by a hose.

Computational Methods. The calculations were performed with the Gaussian 03 package.[9] The starting molecular geometries were obtained at the HF/3−21G level of theory. The final molecular geometry optimizations were performed with the Kohn−Sham DFT.[10] The Becke three-parameter hybrid exchange-correlation function (B3LYP[11]) was used with the pseudopotential basis set LanL2DZ.[12] No symmetry condition was imposed. Vibrational frequencies were calculated from the analytic second derivatives to check the minimum on the potential energy surface.

Molecular orbital (MO) compositions and the overlap populations were calculated using the AOMix program.[13]

Time-dependent density functional theory (TDDFT) was used to calculate the energies and intensities of electronic transitions.[14,15]

(6) (a) Carlos, R. M.; Carlos, I. A; Neumann, M. G. *Inorg. Chim. Acta* **2000**, *299*, 231–237. (b) Pereira, C.; Ferreira, H. G.; Schultz, M. S.; Milanez, J.; Izidoro, M.; Leme, P. C.; Santos, R. H. A.; Gambardella, M. T. P.; Castellano, E. E.; Lima-Neto, B. S.; Carlos, R. M. *Inorg. Chim. Acta* **2005**, *358*, 3735–3744.

(7) Carlos, R. M.; Neumann, M. G. *J. Photochem. Photobiol.* **2000**, *131*, 67–73.

(8) Calvert, J. G.; Pitts, J. N. *Photochemistry*, 2nd ed.; Wiley: New York, 1967; pp 779−789.

(9) Frisch M. J.; Trucks, G. W.; Schlegel, H. B.; Scuseria, G. E.; Robb, M. A.; Cheeseman, J. R.; Montgomery, J. A., Jr.; Vreven, T.; Kudin, K. N.; Burant, J. C.; Millam, J. M.; Iyengar, S. S.; Tomasi, J.; Barone, V.; Mennucci, B.; Cossi, M.; Scalmani, G.; Rega, N.; Petersson, G. A.; Nakatsuji, H.; Hada, M.; Ehara, M.; Toyota, K.; Fukuda, R.; Hasegawa, J.; Ishida, M.; Nakajima, T.; Honda, Y.; Kitao, O.; Nakai, H.; Klene, M.; Li, X.; Knox, J. E.; Hratchian, H. P.; Cross, J. B.; Bakken, V.; Adamo, C.; Jaramillo, J.; Gomperts, R.; Stratmann, R. E.; Yazyev, O.; Austin, A. J.; Cammi, R.; Pomelli, C.; Ochterski, J. W.; Ayala, P. Y.; Morokuma, K.; Voth, G. A.; Salvador, P.; Dannenberg, J. J.; Zakrzewski, V. G.; Dapprich, S.; Daniels, A. D.; Strain, M. C.; Farkas, O.; Malick, D. K.; Rabuck, A. D.; Raghavachari, K.; Foresman, J. B.; Ortiz, J. V.; Cui, Q.; Baboul, A. G.; Clifford, S.; Cioslowski, J.; Stefanov, B. B.; Liu, G.; Liashenko, A.; Piskorz, P.; Komaromi, I.; Martin, R. L.; Fox, D. J.; Keith, T.; Al-Laham, M. A.; Peng, C. Y.; Nanayakkara, A.; Challacombe, M.; Gill, P. M. W.; Johnson, B.; Chen, W.; Wong, M. W.; Gonzalez, C.; Pople, J. A. *Gaussian 03*, Revision C.02; Gaussian, Inc.: Wallingford, CT, 2004.

(10) Kohn, W.; Sham, L. J. *Phys. Rev.* **1965**, *140*, A1133.

(11) Lee, C.; Yang, W.; Parr, R. G. *Phys. Rev.* **1998**, *B37*, 785.

(12) Becke, A. D. *J. Chem. Phys.* **1993**, *98*, 5648.

(13) (a) Gorelsky, S. I. *AOMix: Program for Molecular Orbital Analysis*; York University: Toronto, Canada, 1997; http://www.sg-chem.net. (b) Gorelsky, S. I.; Lever, A. B. P. *J. Organomet. Chem.* **2001**, *635*, 187.

(14) Casida, M. E. In *Recent Advances in Density Functional Methods*; Chong, D. P., Ed.; World Scientific: Singapore, 1995.

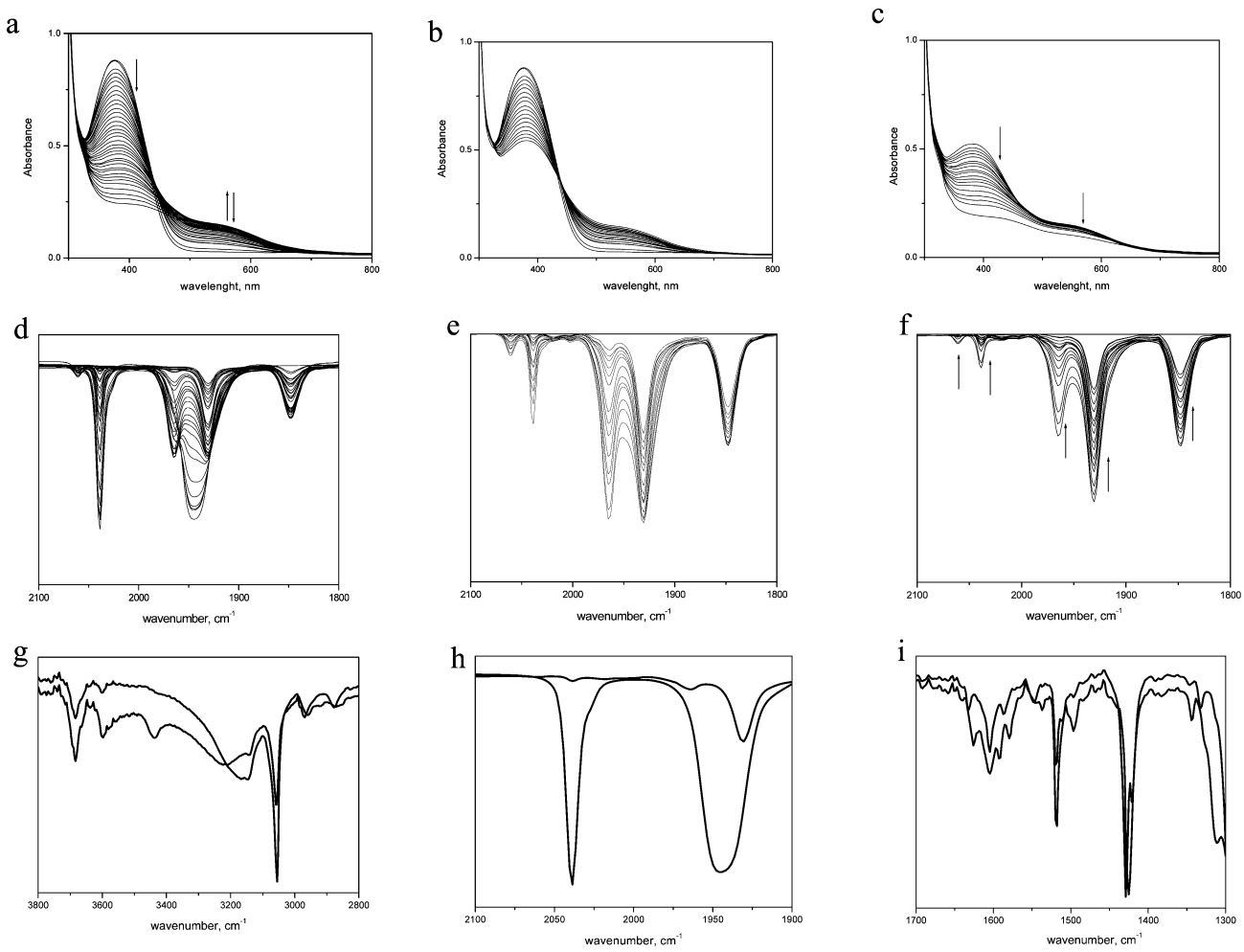

Figure 1. Continuous photolysis of *fac*-**1** with 350 nm light in CH_2Cl_2 solution: (a, b, c) changes in the absorption spectrum, $I_0 = 1 \times 10^{-9}$ einstein s^{-1}, (d,e,f,g,h,i) changes in the FTIR spectra, $I_0 = 1 \times 10^{-7}$ einstein s^{-1}.

The calculated electronic transitions were convoluted using Gaussian functions having half-widths of 25,000 cm^{-1} with the Swizard program.[16]

III. Results and Discussion

The results obtained in the solvents CH_2Cl_2 and CH_3CN are similar. Since the DFT calculations were carried out in CH_2Cl_2, we will give as experimental examples those concerning the manganese complex in this solvent.

Continuous Photolysis Investigations. As noted in an earlier paper,[6] photolysis into the UV−visible absorption band of *fac*-**1** causes an efficient photoreaction, with a quantum yield of 0.60 at $\lambda_{exc} = 350$ nm, converting it into *mer*-**1**. Exhaustive photolysis led to a final stable spectrum. In the present study we have detected the presence of intermediates in the parent complex.

Figure 1a,b,c displays the changes in the UV−vis spectra of a CH_2Cl_2 solution of *fac*-**1** during photolysis using the excitation wavelength 350 nm ($I_0 = 1 \times 10^{-9}$ einstein s^{-1}). In this experiment, after a 10 min photolysis of *fac*-**1**, the irradiation was stopped, and the thermal stability of the solution was monitored by changes in the UV−vis spectrum of the parent complex. After 2 h measurements, the absorption spectrum did not change (Figure 1b). Further irradiation caused more depletion of the parent complex with the same increases in the intensity of the new band found before. It grew at the same rate during the course of the experiment indicating the formation of a single species. However, after 20 measurements a depletion of the maximum absorption of the *mer*-**1** species is observed (Figure 1c).

Photolysis of *fac*-**1** with 350 nm light $I_0 = 1 \times 10^{-7}$ einstein s^{-1} was also monitored in situ by FTIR spectroscopy. Upon irradiation, the two ν(CO) bands from *fac*-**1** at 2037 cm^{-1} and 1940 cm^{-1} decrease in intensity. New absorptions initially grow at 1965 and 1931 cm^{-1}. These new ν(CO) bands are attributed to the *mer*-**1** isomer (Figure 1d). Apart from the *mer*-**1** absorption bands, two new absorptions at 2065 and 1890 cm^{-1} appear. First increasing in intensity and then decaying in the first 320 s of irradiation (Figure 1e,f). Particularly, the imidazole proton is dissociated during the photoreaction producing a new absorption at 3219 cm^{-1} (Figure 1g). The phenanthroline anion (phen$^{\bullet-}$) modes found at 1312, 1345, 1429, 1496 1537, 1576, 1604 cm^{-1} were seen

(15) Stratmann, R. E.; Scuseria, G. E.; Frisch, M. J. *J. Chem. Phys.* **1998**, *109*, 8218.

(16) Gorelsky, S. I. *Swizard*; Department of Chemistry, York University: Toronto, ON, 1999; http://www.sg-chem.net.

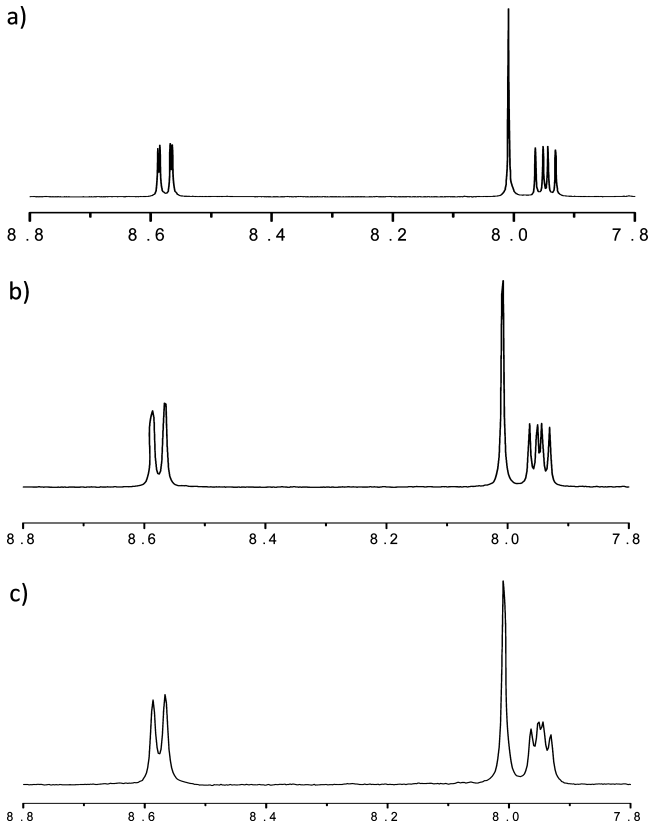

Figure 2. Three phenanthroline peaks of NMR spectrum in CD_2Cl_2 solution for *fac*-**1** at different times of irradiation: $a = 0$ s, $b = 30$ s, $c = 90$ s.

as in reasonable agreement with the literature values[17] (Figure 1i).

The course of the photochemical reaction of *fac*-**1** was also studied by ^{1}H NMR. A CD_2Cl_2 solution of *fac*-$[Mn(CO)_3(phen)(imH)]^+$ was irradiated at room temperature with 350 nm radiation ($[fac\text{-}\mathbf{1}] = 2.3 \times 10^{-2}$ mol L^{-1}, $I_0 = 1 \times 10^{-7}$ einstein s^{-1}) and the proton NMR taken at appropriate intervals. Two spectra are shown in Supporting Information, Figure S1. Simple intensity arguments tell us that the four peaks with shifts between 8.0 ppm and 9.6 ppm are from the phenanthroline protons. The three peaks from 6.5 ppm to 6.9 ppm are the three ring protons of imidazole. This has been confirmed by a COSY experiment. The broad peak at 11.5 ppm is the N−H proton of the imidazole ligand. The peak at 5.2 ppm is the $CHDCCl_2$ peak from the solvent, and the large broad line at 1.6 ppm is H_2O. Only two things in the spectra change with increasing time of radiation. One is the line width of all peaks, including the solvent and water peaks. In Figure 2 is shown just the portion of the spectra pointing out three of the four phenanthroline proton peaks. The change in line width in Figure 2 is from 0.7 Hz to about 10 Hz, a change of over one magnitude. Besides the width changes, there is no change in chemical shifts and no change in the relative magnitudes of the phenanthroline and imidazole peaks.

The second change is in the relative intensity of the solvent peak to the *fac*-**1** peaks, that increases with increasing radiation time. Since the total intensity of the solvent peak remains constant, the concentration of *fac*-**1** must be decreasing with time. Using the relative ratio of the area of the solvent peak to the area of the 9.6 ppm peak from the phenanthroline ligand, we noted that the concentration of *fac*-**1** decreases linearly with time. After 110 s of irradiation, it reaches half of the starting concentration. Imidazole N−H deprotonation was also detected by ^{1}H NMR.

The data suggests that the photolysis of *fac*-**1** is converting it into a paramagnetic molecule.

Flash Photolysis Studies. Insight into the events following the 355 nm photolysis of the *fac*-**1** complex was provided by examination of the absorption UV−vis spectral changes on the nanoseconds time scale. Preliminary transient absorption experiments in deoxygenated solution were compromised by the net photochemistry. To avoid flash photolysis of secondary products, fresh solutions of *fac*-**1** (4.0 mL) were flashed once (one transient trace taken) and then the solution was replaced by a new one.

Readily apparent spectral changes are a strong transient bleaching at 370 nm close to the maximum of the ground-state lowest-energy absorption band of *fac*-**1**, and a strong absorption at 610 nm characteristic of the phen$^{\bullet-}$ (Figure 3a). DFT calculations (see below) predict two charge transfer transitions in this region: metal-to-ligand charge-transfer (MLCT, Mn→phen) and ligand-to-ligand charge-transfer (LLCT, im→phen). The Δabs versus time profiles at 370 nm (transient bleaching) and at 610 nm (transient absorption) are shown in Figure 3b,e. Both traces did not return to baseline, but led to residual bleaching with a long lifetime. The decay of the 370 nm transient could be fit to a simple exponential decay ($\tau_1 = 2.3 \times 10^{-7}$ s). At $\lambda_{monitored} = 610$ nm the initial bleach evolved into a transient absorbance with a much slower lifetime and could be fitted to a second-order rate constant ($\tau_2 = 4.53 \times 10^{-7}$ s (80%) and $\tau_3 = 8.55 \times 10^{-8}$ s (20%)) (Figure 3e). The lack of room temperature emission[6] for *fac*-**1** suggests that short lifetime component belongs to the ^{3}MLCT (Mn→phen) excited states populated by direct excitation of the corresponding ^{1}MLCT states.

Besides the excited-state bands, new transient absorptions characterized by apparent maxima at 480 and 510 nm were observed. They appear to encompass two absorption bands (Figure 3a). These absorptions can be attributed to the formation of an imidazole radical.[18] The data related to the strong absorption at 480 nm could not be fitted satisfactorily to single exponential decays. However, the data give good mathematical fits (correlation constants >0.90) for a model involving two parallel exponential decays with different lifetimes ($\tau_3 = 1 \times 10^{-6}$ s, 87% and $\tau_4 = 1 \times 10^{-8}$ s, 12%). The slower component represents the dominant absorbance changes at this wavelength (Figure 3c,d). The τ_3 and τ_4 represent the decays of two transient species generated within the time scale of the laser flash, leading to the same product (A → C and B → C, where C is *mer*-**1**) or, possibly, to two different species of closely similar spectra. The transient absorption lifetime at 510 nm (1.16×10^{-8} s) was exactly

(17) (a) Turro, C.; Chung, Y. C.; Leventis, N.; Kuchenmeister, M. E.; Wagner, P. J.; Leroi, G. E. *Inorg. Chem.* **1996**, *35*, 5104–5106. (b) Howell, S. L.; Gordon, K. C. *J. Phys. Chem.* **2004**, *108*, 2536–2544.

(18) Riem, R. H.; McLachlan, A.; Coraor, G. R.; Urban, E. J. *J. Org. Chem.* **1971**, *36*, 2272–2275.

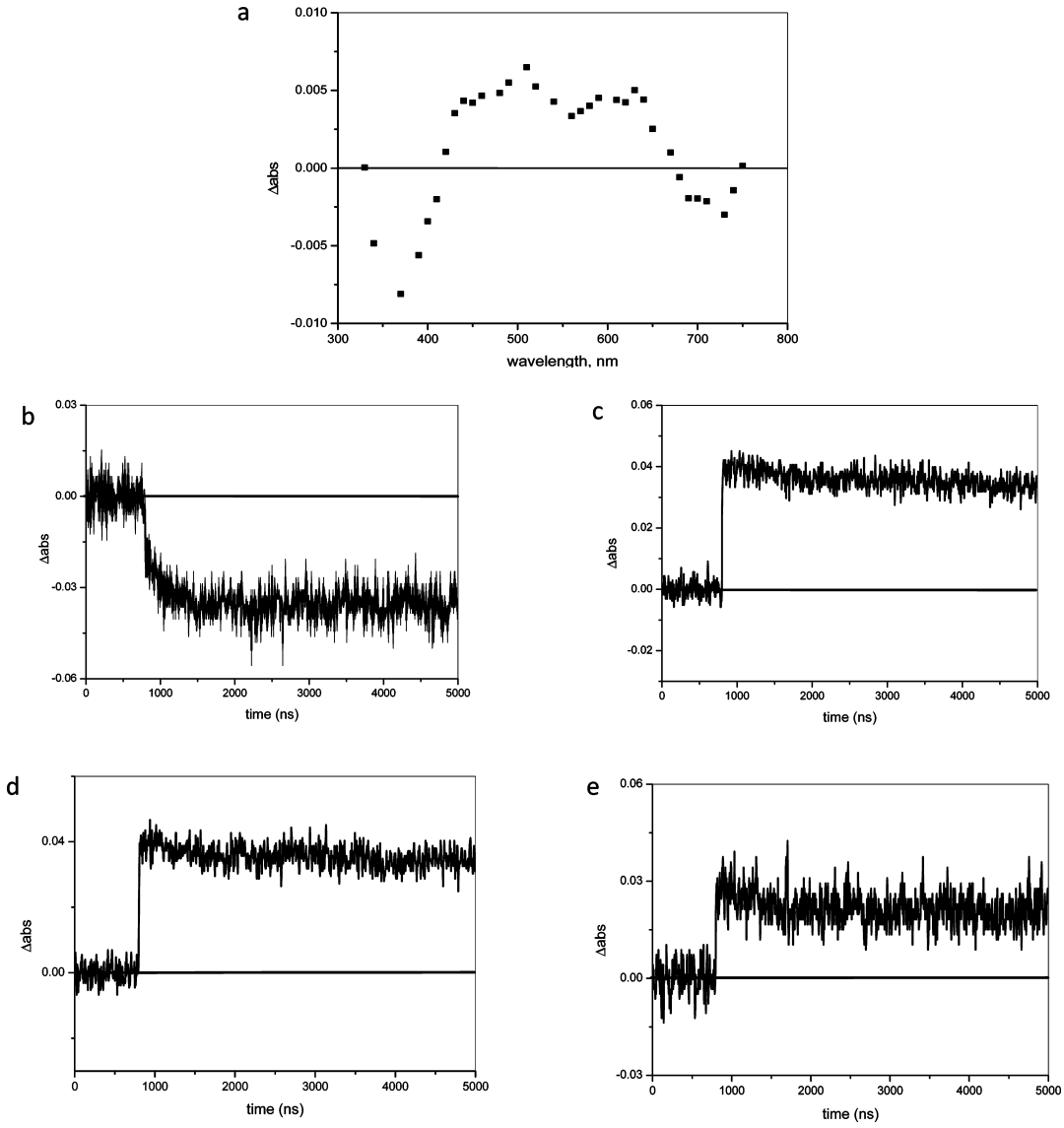

Figure 3. (a) Difference spectrum of *fac*-**1** in CH_2Cl_2 solution measured 8 ns after 355 nm laser excitation. *fac*-**1** (10 μmol L^{-1}). (b,c,d,e) Absorption changes following 355 nm flash photolysis of *fac*-**1** in CH_2Cl_2 solution monitored at (b) 390nm, (c) 480 nm, (d) 510 nm, and (e) 610 nm.

matched by the short component at 480 nm, both traces fitting well to first-order kinetics (Figure 3d).

Photoinduced Electron Transfer Reactions. To provide support for the photochemical results, *N*,*N*-dimethyl-4,4′-bipyridinium chloride (MV^{2+}) was introduced as a trap for any "intermediate key" produced during the photolysis of *fac*-**1**. In this experiment, about 10-fold excess of methyl viologen (MV^{2+}) was added into a $\sim 1 \times 10^{-4}$ mol L^{-1} complex in deoxygenated acetonitrile solution. The intermolecular electron transfer reaction was followed by the transient absorption spectrum. Before irradiation, the absorption spectrum of the mixture exhibits the characteristic absorption of *fac*-**1** at 380 nm (yellow solution). Upon flash excitation at 350 nm the solution turned blue because of the rapid appearance of the $MV^{\bullet+}$ radical. The transient absorption spectrum depicted the appearance of the $MV^{\bullet+}$ radical around 390 and 610 nm[19] and the decrease of the absorption at 480 nm. The rate of the transient decay (480 nm) decreased nearly 300 times from 1×10^{-6} s in the absence of MV^{2+} to 3×10^{-9} s in its presence. The absorptions at 610 nm increased from 1×10^{-7} to 3×10^{-7} s.

Figure 4a shows the UV−vis absorption spectral change of the reaction solution containing *fac*-[Mn(CO)$_3$(phen)(Him)]$^+$ and MV^{2+} before photolysis (a), immediately after photolysis (b), and during the disappearance of the $MV^{\bullet+}$ absorption by thermal reaction (c). In the first spectrum (a) solution of *fac*-[Mn(CO)$_3$(phen)(Him)]$^+$ with MV^{2+} (yellow solution) was excited at 355 nm. A broad absorption band with maxima near 605 and a peak at 394 nm appeared just after irradiation commenced (b). These new absorptions closely match the methyl viologen radical ($MV^{\bullet+}$) absorption spectrum (blue solution). The subsequent $MV^{\bullet+}$ consume by thermal back electron transfer reaction to give MV^{2+} and manganese "products" was followed by changes in the

(19) (a) Kosower, E. M.; Cotter, J. L. *J. Am. Chem. Soc.* **1964**, *86*, 5524–5527. (b) Watanabe, T.; Honda, K. *J. Phys. Chem.* **1982**, *86*, 2617–2619.

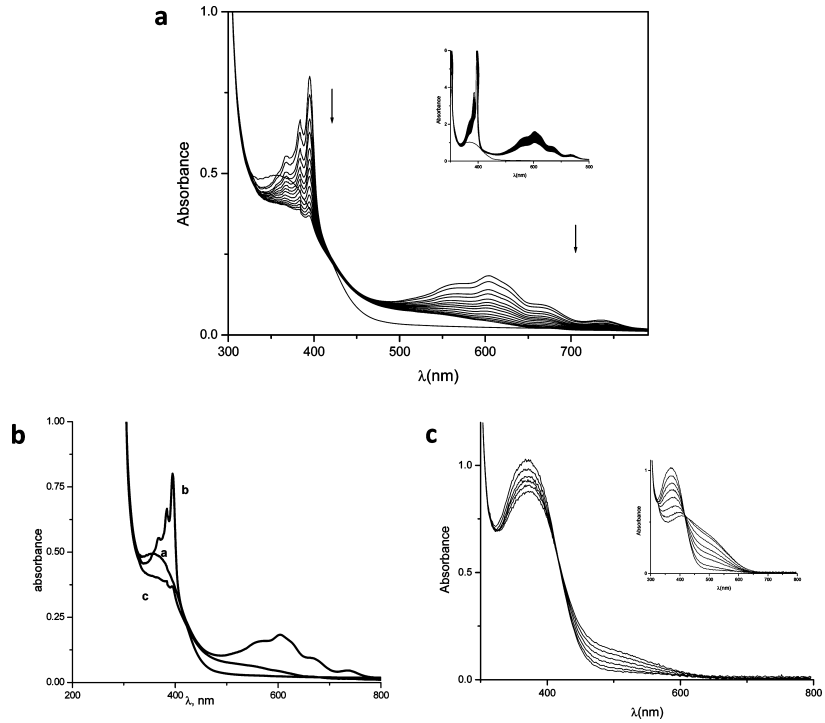

Figure 4. (a) Absorption spectra of *fac*-$[Mn(CO)_3(phen)(Him)]^+$ and MV^{2+} in CH_3CN. Inset: absorption spectra obtained during the thermal back reaction in a very concentrated solution of MV^{2+}. (b) Absorption spectra of the *fac*-$[Mn(CO)_3(phen)(Him)]^+$ and MV^{2+} in CH_3CN: (a) before irradiation; (b) immediately after irradiation; (c) after the back thermal reaction. The excitation source was a Nd:YAG laser (355 nm). (c) Absorption spectra obtained during continuous photolysis of *fac*-$[Mn(CO)_3(phen)(Him)]^+$ in CH_3CN solution. Inset: Absorption spectra after 20 measurements.

UV−vis absorption spectrum of the reduced $MV^{\bullet+}$ (Figure 4a). The UV−vis spectra monitored during the slow (45 min) thermal back reaction exhibited isosbestic conversion at 426 nm. This experiment has been repeated for a different concentration of MV^{2+} resulting in the same kind of behavior (Figure 4a, inset).

For comparison a CH_3CN solution of *fac*-$[Mn(CO)_3(phen)(imH)]^+$ alone was irradiated at room temperature with 350 nm radiation ([*fac*-**1**] = 2.3×10^{-2} mol L^{-1}, $I_0 = 1 \times 10^{-7}$ einstein s^{-1}). The absorption spectrum was taken at appropriate intervals. Two spectra are shown in Figure 4c. Readily apparent spectral changes are the continuous depletion of the *fac*-$[Mn(CO)_3(phen)(Him)]^+$ absorption with increases in the intensity of the 560 nm band. The spectral changes are accompanied by isosbestics conversion at 426 nm (Figure 4c). Notably the spectrum measured over a period of seconds after the initiation of the reaction was similar to that obtained in Figure 4b (spectrum c).

Figure 4c (inset) shows that further irradiation caused more depletion of the *fac*-$[Mn(CO)_3(phen)(Him)]^+$ complex with increases in the intensity of the 560 nm band found before and what grew in the course of the experiment. However, the isosbestics conversion is not observed anymore indicating two different species of closely similar spectra.

On the basis of these outcomes, the blue color photoproduct is proposed to result from an electron transfer reaction, one electron being transferred from the long-lived intermediate to the viologen moiety. In this experiment the parent complex is not regenerated at all. In the conditions pointed out in Figure 4a, the cyclic process can be repeated twice.

Theoretical Studies. For the interpretation of all the photochemical results presented for *fac*-**1**, the character of the orbitals involved in the electronic transitions and the nature of the lowest excited states of these complexes have to be considered. DFT calculations were performed on the complexes *fac*-$[Mn(CO)_3(phen)(Him)]^+$ (*fac*-**1**), *mer*-$[Mn(CO)_3(phen)(Him)]^+$ (*mer*-**1**), and *mer*-$[Mn(CO)_3(phen)(im^{\bullet-})]^+$ (*mer*-**1**$^\bullet$). The general view of the equilibrium structures and the main calculated bond lengths of complexes are given in Supporting Information, Figure S2 and Supporting Information, Table S1.

The *fac*-**1** complex has C_s symmetry with the atoms CO, Mn, and N of the equatorial phenanthroline ligand lying on the same plane of symmetry. Both *mer*-**1** and *mer*-**1**$^\bullet$ complexes have similar structures defined with the (CO)C−Mn−C(CO) in the z axis of the C_s molecule. The coordination around the central Mn atom is nearly octahedral. For *fac*-**1** complex, the polyhedron is distorted with the trans $N_{23}-Mn-C_4$ angle of 173.8° and (phen)N−Mn−N(phen) of 79.4°. The optimized geometry data are in good agreement with the experimental X-ray parameters for the related manganese complexes[6] *fac*-$[Mn(CO)_3(phen)L]^+$, L = isn, SO_3CF_3, H_2O.

Upon *fac*-**1** to *mer*-**1** structural rearrangement, the $(phen)N_{14}-Mn-N_8(imH)$ and the $C_4(CO)-Mn-N_{23}(phen)$ angles increase 5.3° and 3.2°, respectively. The imidazole moiety is twisted 63.3° out of the phenanthroline plane.

The main deformations after deprotonation of the imidazole ring are a decrease of the $(CO)C_{16}-Mn-N_{17}(im)$ angle from 4.1° and an increase of the $N_{17}(im)-Mn-N_2(phen)$ and

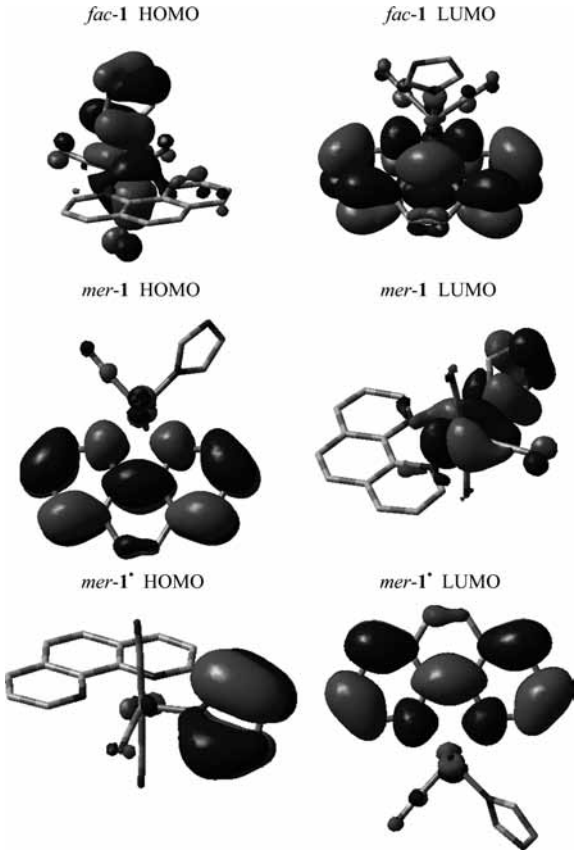

Figure 5. Contour surfaces of frontier molecular orbital of *fac*-**1**, *mer*-**1**, and *mer*-**1**•.

N_{17}(im)−Mn−N_3(phen) angles of about 5°. The calculated Mn−C16(CO) bond lengths are higher, by 0.118 Å, than that found for *mer*-**1**, while the Mn−N_{17}(im) bond distances are shorter by 0.126 Å.

It is relevant that the π-acceptor ability of CO does not determine such structural features. Indeed, if the back-bonding effect was significant, the Mn−CO bonds in *mer*-**1** should be longer than those in *fac*-**1** because of destabilization of the *trans*-CO−Mn−CO fragment with two effective π-acceptores. However, the C≡O bonds are almost the same for all the isomers.

Molecular Orbital Analysis. The energies and composition of the frontier molecular orbital of complexes *fac*-**1**, mer-**1**, and *mer*-**1**•, are given in Supporting Information, Table S2. Their representations are depicted in Figure 5.

In *fac*-**1**, most of the electron density is shared between the manganese d-orbital in character (66%) and imidazole (33%). The highest occupied molecular orbital HOMO-1 is predominantly imidazole π orbitals. The HOMO-2, -3, and -4 are found at almost the same energy as HOMO-1 and are composed of π bonding phen, imidazole, and *d* Mn.

The lowest unoccupied molecular orbital (LUMO) and LUMO+1 are essentially π orbitals of the phen moieties (Figure 5a). The following three mostly Mn ($d_{x^2-y^2}$ and d_{z^2}) orbitals and CO π^* are still higher in energy and display bonding (LUMO+2, −2.74 eV; LUMO+3, −2.26 eV; and LUMO+4, −2.14 eV) or antibonding (LUMO+5, −1.85 eV; and LUMO+6, −1.64 eV) interactions with the ligands.

From the energies listed, we note that there is a HOMO−LUMO gap of 2.35 eV. Considering the correlation between energy and degree of charge delocalization it is found that the Mn-phen covalent interaction involves charge-donation from the {Mn(CO)$_3$imH}$^+$ fragment to the phen ligand in agreement with the experimental results.

The *fac*-**1** to *mer*-**1** structural changes have a pronounced effect on the energy and composition of the frontier molecular orbitals. The phen ligand participates in more than 90% of this orbital. Its energy is 1.58 eV shorter than the corresponding HOMO of the *fac*-**1** isomer (Supporting Information, Table S2, Figure 5). So, in addition to MLCT (Mn→phen) and LLCT (im→phen) bands in the electronic spectra of these complexes, we can also expect LMCT (phen→Mn) and ILCT (phen→phen) transitions. Also, the HOMO−LUMO gap found for *mer*-**1** is shorter than that observed for the *fac*-**1** complex. It is in qualitative agreement with the lower-energy shift of the HOMO−LUMO transition by some 8000 cm^{-1} that is observed experimentally (Figure 1a).

When the imidazole is deprotonated, as it is observed during photolysis (shown in the previous section), the electron density resides mainly on the imidazole ligand (97%). It is to note that deprotonation leads to an energy increase of this orbital to a value close to that found for *fac*-**1**, the thermodynamically more stable species.

The HOMO−LUMO gap decreases in the order *mer*-**1**• (3.54 eV) > *fac*-**1** (2.36 eV) > *mer*-**1** (1.41 eV). The smallest value noted for *mer*-**1** complex indicates the destabilization of the HOMO on the phenanthroline ligand, thus making the imidazole ligand easier to oxidize and the *mer*-**1**• species more stable.

Electronic Absorption Spectra Studies. The experimental and calculated absorption spectrum data of *fac*-**1** and *mer*-**1** are reported in the Supporting Information, Table S3. The theoretical data reproduce reasonable well the energetic position (within 0.15 eV) and the intensities of the absorption bands in the electronic spectrum of complexes.

The calculations indicate that the broad absorption with a maximum at 361 nm in the spectrum of *fac*-**1** is LLCT (im→phen, 3.43 eV) in character (Supporting Information, Table S3). The next lowest energy excited states are the ILCT (phen→phen*, 3.50). The energy difference between these transitions, 0.07 eV, is not significant although the difference in calculated intensity is large ($f = 28-63 \times 10^{-4}$). The MLCT (Mn→ phen) transition is found at lower energies (3.01 eV) and exhibits much smaller oscillator strengths (2×10^{-4}). The relative ordering of these states can thus be summarized as MLCT (Mn→ phen, 3.01 eV) < LLCT (im→phen, 3.43 eV) < ILCT (phen→phen* 3.50).

In *mer*-**1**, the MLCT (Mn→phen, 2.41 eV, 515 nm) transitions lie close in energy to the LLCT (im→phen, 2.47 eV, 502 nm).

The results obtained for *fac*-**1** differ from those presented for the homologous complex *fac*-[Re(phen)(imH)(CO)$_3$]$^+$.[20] The emissive lowest-lying excited-state in *fac*-[Re(phen)(imH)(CO)$_3$]$^+$originates from the ^{3}MLCT (Re→phen) lowest-lying excited state. The photochemical properties found for *fac*-**1**

can be attributed to the small size and larger charge of the manganese center. It enforces ionic bonding and allows a better approach of the σ-donor ligand imidazole compared to Re^{I}, where the size of the cation is larger. The change sufficiently affects the excited-state character to switch the photochemical mode. Therefore, the LLCT states are expected to occur at energies close to the lowest MLCT state. It explains the photochemical activity of the manganese complex. The excitation induces a strong charge shift from both the axial imidazole ligand and the manganese center to the equatorial phen ligand, without any weakening of Mn-ligand bond. In consequence, the charge of the axial imH ligand and manganese(II) decreases and those of the equatorial phen and CO ligands increase. The latter change may be effective in promoting the *fac*- to *mer*-isomerization. It may also substantiate the deprotonation of the imidazole ligand. Additionally, in the Re complexes it is not unreasonable to assume that the observable absorptions include substantial singlet triplet character whereas the Mn complexes do not.[21]

A system sensitive enough to respond photochemically to the subtle changes in ligand nature could be found within the same manganese family, when ligand L is not changed but only slightly modified. These studies are underway in our laboratory.

Conclusion

In the preceding sections, the structure, spectroscopy, and excited state dynamics of the *fac*-**1** to *mer*-**1** photochemical induced isomerization have been described. The MO calculations on the *fac*-**1**, *mer*-**1**, and *mer*-**1**$^{\bullet}$ show the strong electron donation from the imidazole and manganese center toward the phenanthroline ligand, and the extensive mixing of the σ imidazole and manganese π orbitals in the HOMO and phen π^* orbitals in the LUMO. These electronic features are responsible for the unusual stability and long lifetime of the intermediates species and its spectroscopic and redox consequences. This effect is well documented by the flash photolysis and quenching experiments.

Acknowledgment. The authors would like to acknowledge the financial support from FAPESP, CAPES, and CNPq. They are also indebted to Dr. Edson Rodrigues from IQSC-USP for his helpful discussions.

Supporting Information Available: Figures S1, S2 and Tables S1−S3. This material is available free of charge via the Internet at http://pubs.acs.org.

IC8002004

(20) (a) Connick, W. B.; DiBilio, A. J.; Hill, M. G.; Winkler, J. R.; Gray, H. B. *Inorg. Chim. Acta* **1995**, *240*, 169–173. (b) Di Bilio, A. J.; Crane, B. R.; Wehbi, W. A.; Kiser, C. N.; Abu-Omar, M. M.; Carlos, R. M.; Richards, J. H.; Winkler, J. R.; Gray, H. B. *J. Am. Chem. Soc.* **2001**, *123*, 3181–3182. (c) Busby, M.; Gabrielsson, A.; Matousek, P.; Towrie, M.; Di Bilio, A. J.; Gray, H. B.; Vlcek, A. *Inorg. Chem.* **2004**, *43*, 4994–5002.

(21) Wrighton, M. S.; Morse, D. L.; Gray, H. B.; Ottesen, D. K. *J. Am. Chem. Soc.* **1976**, *98*, 1111–1119.